

Resilience of mobility network to dynamic population response across COVID-19 interventions: evidences from Chile

Pasquale Casaburi^{1,2}, Lorenzo Dall’Amico¹, Nicolò Gozzi¹, Kyriaki Kalimeri¹, Anna Sapienza^{3,1}, Rossano Schifanella^{1,4}, T. Di Matteo^{2,5,6}, Leo Ferres^{7,1}, Mattia Mazzoli¹

¹ ISI Foundation, via Chisola 5, 10126 Turin, Italy

² Department of Mathematics, King’s College London, The Strand, London WC2R 2LS, UK

³ Università del Piemonte Orientale, V.le Teresa Michel, 11, 15121 Alessandria, Italy

⁴ Università degli Studi di Torino, Turin, Italy

⁵ Complexity Science Hub Vienna, Josefstädter Straße 39, 1080 Vienna, Austria

⁶ Museo Storico della Fisica e Centro Studi e Ricerche Enrico Fermi,
Via Panisperna 89A, 00184 Rome, Italy

⁷ Universidad del Desarrollo, Santiago de Chile, Chile

Abstract

Background The COVID-19 pandemic highlighted the importance of non-traditional data sources, such as mobile phone data, to inform effective public health interventions and monitor adherence to such measures. Previous studies showed how socioeconomic characteristics shaped population response during restrictions and how repeated interventions eroded adherence over time. Less is known about how different population strata changed their response to repeated interventions and how this impacted the resulting mobility network.

Methods We study population response during the first and second infection waves of the COVID-19 pandemic in Chile and Spain. Via spatial lag and regression models, we investigate the adherence to mobility interventions at the municipality level in Chile, highlighting the significant role of wealth, labor structure, COVID-19 incidence, and network metrics characterizing business-as-usual municipality connectivity in shaping mobility changes during the two waves. We assess network structural similarities in the two periods by defining mobility hotspots and traveling probabilities in the two countries. As a proof of concept, we simulate and compare outcomes of an epidemic diffusion occurring in the two waves.

Results While differences exist between factors associated with mobility reduction across waves in Chile, underscoring the dynamic nature of population response, our analysis reveals the resilience of the mobility network across the two waves. We test the robustness of our findings recovering similar results for Spain. Finally, epidemic modeling suggests that historical mobility data from past waves can be leveraged to inform future disease spatial invasion models in repeated interventions.

Conclusions This study highlights the value of historical mobile phone data for building pandemic preparedness and lessens the need for real-time data streams for risk assessment and outbreak response. Our work provides valuable insights into the complex interplay of factors driving mobility across repeated interventions, aiding in developing targeted mitigation strategies.

Introduction

The COVID-19 pandemic has significantly impacted people’s social and behavioral lifestyles worldwide [1–3]. Indeed, people’s routines were affected by government-imposed restrictions aimed at mitigating the virus spread, as well as by individual decision-making processes [4–6]. In both cases, adherence to non-pharmaceutical interventions (NPIs) varied significantly across the population and it was shaped by several factors, including social, demographic, economic variables, and epidemiological conditions [5, 7–9]. Historically, mobility data have been largely leveraged to inform spatial transmission models and perform importation risk assessment in such a complex framework [10–14]. In this context, large-scale mobility datasets became critical non-traditional tools routinely employed to measure and analyze

the effects of non-pharmaceutical interventions (NPIs) aimed at curbing the spread of SARS-CoV-2 on individual behaviors [15–19].

This was possible thanks to the wide availability of data from tech giants and telecommunications companies, providing real-time insights into population activity potentially linked to the virus transmission. However, in the post-pandemic era, data accessibility is undermined by the end of Data for Good programs, hampering our capacity to leverage up-to-date data streams. As a result, the lack of data inevitably hinders our capacity to build sustainable tools for pandemic preparedness and to respond to new epidemics in a timely fashion [20]. Given their high value and ability to account for population-level heterogeneities in adherence to public health interventions, it is thus crucial to profit from the historical mobile phone data collected during the pandemic and to explore the possibility of re-using them for future analyses and modeling [21, 22]. There is a critical need to better understand and integrate human behavioral change into our models to better inform future population-tailored strategies.

Previous works studied the resilience of mobility patterns following shocks, such as extreme weather events [23, 24], epidemics [2, 25–27] or both [28]. Recent findings highlighted how demographic differences were associated to loss of adherence to repeated interventions [29, 30] and to delayed recovery of baseline mobility patterns [26] jointly with local GDP and population density [28], whereas some aspects of individual level visitation patterns were never recovered [2], with different spatial and temporal impacts on urban and rural areas [27]. Recent insights proved that mobility network connectivity of US counties remained almost unaltered during the first COVID-19 wave [21]. However, little is known about how demographic-associated behavioral change due to repeated interventions may have impacted the resulting mobility network structure, and this effect must be quantified.

In this study, we harness large-scale mobile phone data from Chile and Spain, two countries with different social segregation located on two different continents, collected during the COVID-19 pandemic in a consistent fashion. First, we characterize the changes in the mobility response of Chilean municipalities to interventions issued during the first and second waves of COVID-19 by relying, on top of the variables already considered in the literature (such as wealth, labor structure, and demographics), on additional metrics derived from the baseline mobility network. Our results suggest consistency of most factors across waves despite the variability of a few others. We perform a network analysis to characterize the mobility network’s resilience to interventions during the two COVID-19 waves in Chile and Spain. Relying on epidemic modeling, we explore the possibility of reusing historical mobility data to inform disease spatial invasion models of new epidemics.

Our findings represent a step towards enhancing pandemic preparedness by enabling the re-use of non-traditional data sources, like mobile phone data, for predicting population response in health emergencies. Our work sheds light on the dynamic nature of population behavioral change to repeated interventions [29–31], and contributes to the design of tailored public health policies in response to infectious diseases.

Materials and Methods

Mobility data in Chile

On Wednesday, March 18, 2020, the Government of Chile announced the State of Alarm [32], issuing non-pharmaceutical interventions (NPIs) as school closures and mobility restrictions on a set of municipalities, followed by further measures in the next weeks. The country passed to a tiered system of NPIs in July 2020 [33], but a fast resurgence of COVID-19 cases led the Government to announce a tightening of mobility restrictions on all regions on April 1, 2021 [34]. For readability, we define the first two weeks of March 2020 as the *baseline* period, b , representing the “business as usual” mobility network. We let f be the *first wave*, the four weeks following March 16, 2020, and s to be the *second wave*, the four weeks following April 1, 2021. Our study focuses on the weekly average mobility flows in these periods.

Telefónica Chile provided mobility data for Chile in the form of eXtended Detail Records (XDRs). This dataset records the starting time of a data-packet exchange session between a device belonging to an anonymized user and geolocated cell phone towers. The dataset covers the period from March 1, 2020, to April 28, 2021. To minimize noise in the data due to spurious stops not representative of a destination, e.g., devices stopping for a few minutes due to traffic, we defined *stays* as devices connecting to the same tower for at least 30 minutes. We filtered out data points not complying with this condition and obtained a dataset representing users’ *stays*. We assigned cell towers to *comunas* (Chilean municipalities) using their coordinates, and we counted as *trips* all devices switching to a new tower placed at least 500 meters away. We discarded trips between two towers placed within the same municipalities; here, we

only focused on external mobility.

Mobility data in Spain

A national mobile phone operator collected mobility data for Spain, treated [35] and published by the Ministry of Transport, Mobility and Urban Agenda of Spain, *MITMA* in a public and online repository [36]. The data describe the daily movements of individuals between Spanish municipalities from February 21, 2020, to March 18, 2021. Municipalities are mapped into a coarser spatial division in which small rural municipalities with low population density are grouped to include areas not covered by antennas [35]. This data collection is based on individuals’ active events, e.g., users’ calls, together with passive events, in which the user’s device position is registered due to changes in the cell tower of connection. Similarly to the data treatment we performed for Chile, these trips were aggregated using users’ movements between consecutive *stays* of at least 20 minutes in the same area, disregarding trips of less than 500 meters [35]. Here, we focus on external mobility. Hence, we discarded all records regarding trips within the same municipality, i.e., the diagonal of the OD matrices.

Sociodemographic, epidemiological and mobility network metrics for Chile

Chile is characterized by a high level of disparity in socio-economical traits, a high variability of climate conditions from North to South, and a strong urban-rural divide, with the Metropolitan area of Santiago representing the most densely populated area of the country. This is reflected in high heterogeneities of wealth, educational level, median age, active working population, and labor structure across Chilean comunas. In the context of the COVID-19 pandemic, a complex interplay between the above spatial heterogeneities and the epidemic characterized the population response to interventions, with the demographic strata of the population behaving differently. To tackle these differences, we focused on the inter-municipal mobility post-interventions in two separate periods in Chile. Finally, we analyse the resulting mobility network of Chile during the two post-intervention periods and test the validity of our findings in an analogous case study in Spain. We refer the reader to the Supplementary Material for the Spanish case study results and details on the resilience metrics employed.

Specifically for Chile, we collected most of the socio-demographic variables defined at municipality level from the Chilean ‘Instituto Nacional de Estadística’ (INE) [37], while the municipal development index (IDC) was provided by the Universidad Autónoma de Chile (UAC) [38]. The IDC is a composite index that encodes information on the development and welfare of each municipality. Epidemiological data, i.e., confirmed cases, active cases, deaths, and PCR tests by municipality of residence, were collected and made available by the Chilean Ministry of Science [39]. We extracted two variables, namely COVID-19 confirmed cases and PCR tests performed at municipality level, and aggregated these records at a weekly level to minimize noise due to reporting delays and weekends. To better represent the epidemic phases at municipality level, we averaged these data over the four weeks of the two waves periods. We extracted *deaths* records from the database of the *Department of Statistics and Health Information* (DEIS) and the Ministry of Health [40], encoding the number of COVID-19 related deaths in each municipality. See Table 1 for a comprehensive list of all variables collected.

To compare mobility between the first and second wave $\delta^2 M$ defined in Eq. 3, we defined *case increment* as the relative increment of the variable *new cases* between the second and first wave, instead of the incidence of cases.

Mobility Data Analysis

For both countries, we extracted weekly (and daily) origin-destination (OD) matrices $M_{ij,w}$ ($M_{ij,d}$) encoding the total number of trips between municipalities i and j that occurred in week w on day d . These matrices define a time-dependent weighted directed network where nodes are municipalities, links are mobility routes, and link weights are the number of trips occurred in the considered time interval. The weekly aggregated OD matrices will be the main object of study of our work, whereas the daily OD matrices will only serve as a sensitivity test on the time scale of aggregation.

We defined the weekly averaged flows for the three periods as follows:

$$\begin{cases} \bar{M}_{ij,b} = \frac{1}{2} \sum_{w \in b} M_{ij,w}, \\ \bar{M}_{ij,f} = \frac{1}{4} \sum_{w \in f} M_{ij,w}, \\ \bar{M}_{ij,s} = \frac{1}{4} \sum_{w \in s} M_{ij,w}, \end{cases} \quad (1)$$

Variable	Description	Type	Source
log(pop)	logarithm base 10 of the population	static	INE
pop density	population per square meters	static	INE
age	median of the population age	static	INE
urbanization	percentage of population living in urbanized areas	static	INE
gender ratio	number of males divided by the number of females	static	INE
schooling	median of schooling years of the population	static	INE
primary	share of workers employed in the first sector	static	INE
secondary*	share of workers employed in the second sector	static	INE
tertiary	share of workers employed in the tertiary sector	static	INE
dependency	ratio of non-employable over employable population	static	INE
employed	share of employed population (above 15 years old)	static	INE
IDC	municipal development index	static	UAC
new cases	weekly total incidence of COVID-19 new reported cases	dynamic	MinCiencia
active cases*	weekly average incidence of COVID-19 active cases	dynamic	MinCiencia
new deaths	weekly total mortality of COVID-19	dynamic	DEIS
test rate	weekly average of PCR tests per 1000 inhabitants	dynamic	MinCiencia
out-strength pc	S_{out} , baseline out-strength per capita (outbound trips pc)	static	extracted
in-strength pc*	S_{in} , baseline in-strength per capita (inbound trips pc)	static	extracted
out-path-length*	$\langle l_{out} \rangle$, baseline outbound-path-length (peripherality)	static	extracted
in-path-length	$\langle l_{in} \rangle$, baseline inbound-path-length (peripherality)	static	extracted
clustering	c , baseline clustering coeff. (neighbors interdependence)	static	extracted
betweenness	bc , baseline betweenness centrality (key for connectivity)	static	extracted

Table 1: **All variables collected** List of all variables collected in our dataset by description, type, and source. The list includes the socio-economic, epidemiological, and network metrics extracted from the mobility data. *: variable was discarded post VIF test.

We computed for each municipality i the relative outbound mobility drop in the first and second waves with respect to the baseline as:

$$\Delta M_{i,f} = \frac{\sum_{j \neq i} \bar{M}_{ij,f} - \sum_{j \neq i} \bar{M}_{ij,b}}{\sum_{j \neq i} \bar{M}_{ij,b}}, \quad \Delta M_{i,s} = \frac{\sum_{j \neq i} \bar{M}_{ij,s} - \sum_{j \neq i} \bar{M}_{ij,b}}{\sum_{j \neq i} \bar{M}_{ij,b}} \quad (2)$$

Negative values of $\Delta M_{i,f}$ reflect reductions in mobility from the baseline.

Analogously, we defined $\delta^2 M_i$ for each municipality i as the relative change of the total outgoing mobility from i observed during the second wave with respect to the first wave:

$$\delta^2 M_i = \frac{\sum_{j \neq i} \bar{M}_{ij,s} - \sum_{j \neq i} \bar{M}_{ij,f}}{\sum_{j \neq i} \bar{M}_{ij,f}}. \quad (3)$$

Negative values represent lower outgoing flows from municipality i during the second wave with respect to the first wave. To account for municipalities centrality and interdependence in the baseline period ("business as usual") network encoded by $\bar{M}_{ij,b}$, we defined standard network metrics, see Table 1 (we refer the reader to the Supplementary Section *Network metrics* for their mathematical definition).

Regression Model

Spatial lag and linear regression models are performed exclusively on the Chilean case study. First, we measured the Moran index [41] of the mobility drop $\Delta M_{i,P}$ of each Chilean municipality i in Chile in the two periods $P \in \{f, s\}$, first and second wave respectively, to measure the influence of neighboring areas on the mobility change of Chilean *comunas*. We defined spatial proximity of municipalities using a binary Fuzzy contiguity matrix [42, 43] \mathbf{W} , such that $W_{ij} = 1$ if and only if *comunas* i and j are neighbours. We found a Moran index of mobility change in the first wave period of $I_{M_f} = 0.36$ ($p_v < 0.001$) and in the second wave period of $I_{M_s} = 0.22$ ($p_v < 0.001$). Hence, we employed a Spatial Lag model [44] to explain each municipality i outbound mobility drop $\Delta M_{i,P}$ (Eq. 2) from the baseline period in the first and second waves, $P \in \{f, s\}$ respectively. The model takes the general form:

$$\Delta \mathbf{M}_P = \rho \mathbf{W} \Delta \mathbf{M}_P + \beta \mathbf{X}_P + \epsilon \quad (4)$$

where \mathbf{X}_P is the covariates matrix. The model covariates are the baseline mobility network metrics (*e.g.* strength, clustering coefficient, betweenness centrality), sociodemographic variables (*e.g.* population density, gender and age distribution, urbanization level, labor structure), and COVID-related variables (*e.g.* incidence of new cases). As part of the epidemiological variables, the second wave model features two additional covariates, namely the number of deaths and the test rate, that were unavailable in the first wave. We refer the reader to Table 1 for a detailed description of the model variables. Differently from a linear model, an additional term weighted by $\mathbf{W}\Delta\mathbf{M}_P$ takes into account possible spatial autocorrelations, where \mathbf{W} is the spatial proximity matrix defined above. The magnitude of the regression coefficients ρ, β and their statistical significance are computed using a maximum likelihood estimator [43–45]. A statistically significant coefficient ρ means that spatial effects are present and the response of municipalities to NPIs is also influenced by neighbouring areas.

To compare the two different waves, we implemented a linear regression in which the dependent variable is now the relative change of the total outgoing mobility observed during the second wave with respect to the first wave, $\delta^2 M$ defined in Equation 3:

$$\delta^2 \mathbf{M} = \beta \mathbf{X} + \epsilon \quad (5)$$

Where \mathbf{X} is again the covariates matrix. In this case the magnitude and statistical significance of the regression coefficients have been computed using an ordinary least squares estimator.

We standardized the covariates and performed a variance inflation factor test (VIF) [46] to avoid multicollinearity among the covariates. We excluded from all regressions four variables, namely *active cases*, *out-path-length*, *in-strength pc*, and *secondary* as their VIF scored over 10.

Spatial Invasion Model

We define a spatial invasion model on the networks on the first and second wave period, namely $\bar{M}_{ij,f}$, $\bar{M}_{ij,s}$. We simulate an epidemic invasion starting in the municipalities of Santiago Airport in Pudahuel and register the arrival times at municipality level for the next 28 days. We run $n_s = 500$ simulations and compute the average arrival time for each *comuna*, restricting to those who were invaded at least 20 times in all simulations, to compute averages on a minimal sample for each location. The model is a simplified SI (Susceptible-Infected) model in which municipalities can have two states at each time step, $I_m \in \{0, 1\}$, $I_m = 1$ for invaded municipalities and $I_m = 0$ for susceptible ones, we do not account for the internal transmission dynamic. We define the force of invasion from a municipality i on susceptible locations j as:

$$\lambda_{ij} = \beta I_i (1 - I_j) (p_{ij} + p_{ji}) \quad (6)$$

where β defines the probability of infection per contact, $I_i = 1$ and $I_j = 0$ in order to allow for invasion, and p_{ij} and p_{ji} are the traveling probabilities accounting for the mixing of i and j comunas.

Results

Mobility response to interventions in Chile

We focused on Chile’s first and second wave of COVID-19 infections (see Methods for periods definitions). The two intervention periods differed significantly in terms of the number of restricted municipalities and the outbound mobility flows, as shown in Figure 1. While the first month of intervention in the first wave only involved a few *comunas* and had a significant impact on the outbound mobility, the first month of interventions in the second wave had a lower impact on the intensity of outbound mobility flows, despite involving the vast majority of Chilean *comunas*. We hypothesize that municipalities with different demographic profiles, cases incidence, and centrality in the baseline mobility network responded differently to interventions. We investigate the association of socioeconomic, epidemiological, and pre-intervention network metrics with mobility change with respect to the baseline via spatial lag models to account for spatial autocorrelations. Most interestingly, we want to assess whether the response to the second period of interventions was associated with the same factors or if some ceased to explain population response. To do so, we employ a linear regression model to explain the two periods mobility differences.

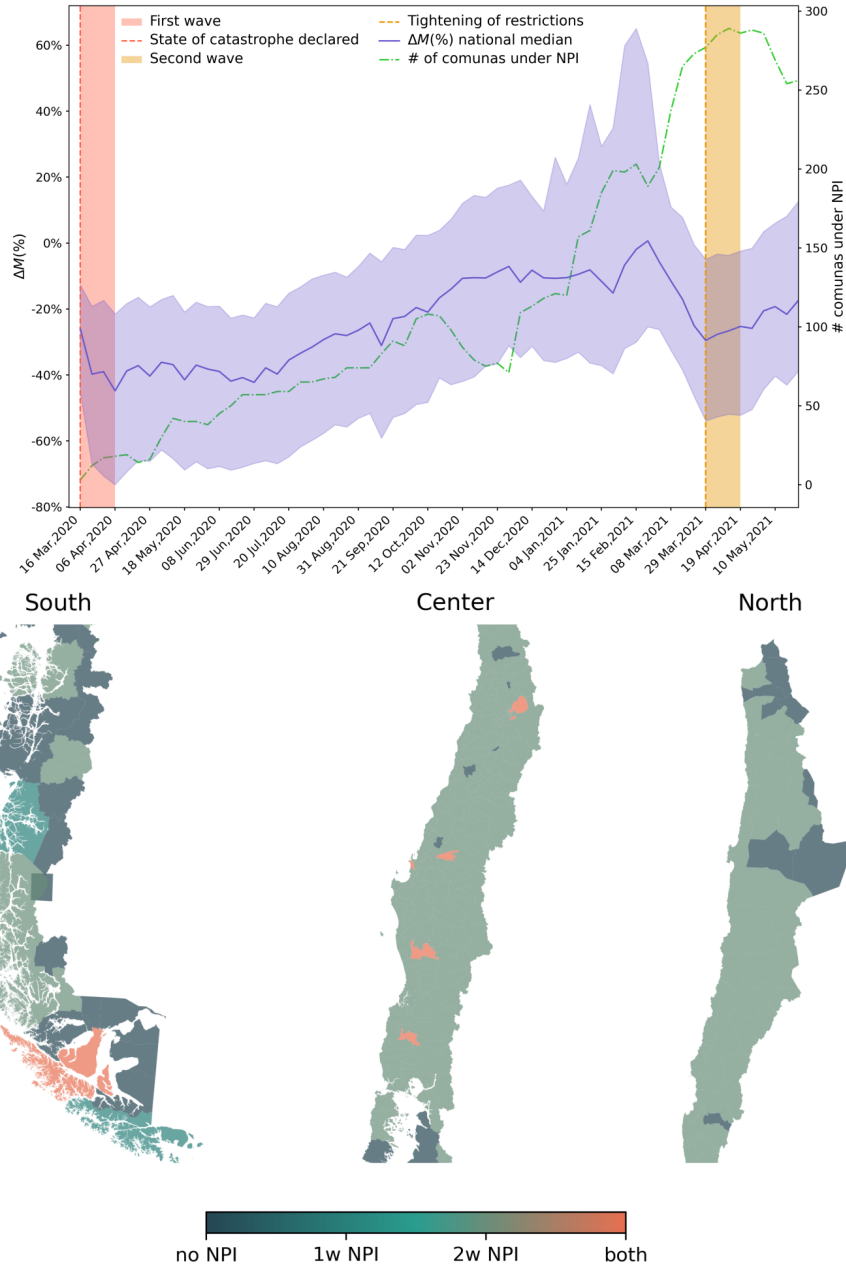


Figure 1: **The first and second wave in Chile.** On top: the weekly median mobility change with respect to baseline, in purple, and respective 95% interval across municipalities as a purple shaded area, dashed green curve as the number of municipalities under restrictions, red shaded vertical area as the first wave period under study and yellow shaded vertical area as the second wave period under study. On the bottom, the map of three macro-regions of Chile shows municipalities under restrictions at any time during the first and second wave periods under study.

First and second COVID-19 waves

The spatial lag model achieves high predictive performance for the first wave in terms of $R^2 = 0.53$ and Kendall Tau, $\tau_K = 0.53$. The detailed results are reported in the left column of Table 2. For some covariates – *e.g.* wealth (encoded as IDC) and labor structure – we recover the results already observed in the literature [7, 9], showing that wealthier municipalities with higher employment in the tertiary sector achieved stronger mobility reductions than others. On top of this, our results enlist additional

variables associated with mobility changes:

- the mobility reduction correlates *positively* with COVID-19 incidence and with the baseline municipalities betweenness centrality;
- the mobility reduction correlates *negatively* with the baseline neighbors' interdependence (*clustering coefficient*), the outbound trips per-capita (*out-strenght pc*) and average peripherality (*path-length*);
- the spatial autocorrelation coefficient is a statistically significant determinant, revealing the importance of municipalities neighbours influence.

	First wave			Second wave			Waves difference		
	Coeff.	[0.025	0.975]	Coeff.	[0.025	0.975]	Coeff.	[0.025	0.975]
intercept	-0.24***	-0.29	-0.21	-0.21***	-0.24	-0.18	-0.0	-0.08	0.08
age	0.01*	0.0	0.03	0.00	-0.02	0.02	-0.21***	-0.32	-0.1
urbanization	0.04***	0.03	0.07	0.06***	0.04	0.09	-0.17*	-0.32	-0.01
gender ratio	-0.01	-0.04	0.0	0.00	-0.02	0.03	0.24**	0.07	0.4
dependency	-0.04***	-0.06	-0.02	-0.07***	-0.1	-0.05	-0.05	-0.22	0.12
schooling	-0.01	-0.04	0.01	0.00	-0.02	0.04	0.12	-0.07	0.31
primary	0.00	-0.02	0.02	-0.03*	-0.07	-0.01	-0.31**	-0.5	-0.12
tertiary	-0.08***	-0.11	-0.06	-0.11***	-0.15	-0.08	0.24*	0.02	0.46
pop density	0.01	-0.01	0.03	0.02*	0.0	0.05	0.12	-0.02	0.25
log(pop)	0.01	-0.01	0.03	-0.01	-0.05	0.01	-0.53***	-0.72	-0.35
IDC	-0.03**	-0.06	-0.01	-0.04*	-0.08	-0.01	0.31**	0.1	0.52
new cases	-0.01**	-0.03	-0.0	-0.00	-0.02	0.01			
clustering	0.02**	0.01	0.05	-0.00	-0.03	0.02	-0.4***	-0.56	-0.24
betweenness	-0.01**	-0.03	-0.0	-0.01	-0.03	0.0	0.06	-0.04	0.16
in-path-length	0.04***	0.03	0.05	0.10***	0.09	0.12	0.18***	0.08	0.27
out-strenght pc	0.03***	0.02	0.05	0.01*	0.0	0.04	-0.25***	-0.35	-0.15
ρ (spatial lag)	0.35***	0.24	0.46	0.19***	0.09	0.3			
deaths				0.00	-0.01	0.01			
test rate				0.00	-0.01	0.02			
cases increment							-0.01	-0.1	0.08
	Pseudo $R^2 = 0.53$ $\tau_K = 0.53$ ***			Pseudo $R^2 = 0.58$ $\tau_K = 0.38$ ***			Adjusted $R^2 = 0.49$ $\tau_K = 0.38$ ***		

Table 2: **Correlates of mobility change across the two waves in Chile.** *Tables in the first and second columns: first and second wave.* The spatial lag model coefficients, β for covariates and ρ for spatial lag from Equation (4) are reported with their 95% confidence interval and the goodness of fit measured by R^2 and the Kendall's Tau (τ_K) coefficient between observed and predicted mobility drops. *Table in the third column: comparison between waves.* Linear regression coefficients β and respective 95% confidence interval for the model of Equation (5). For all models, the goodness of fit is reported at the bottom of the table, and we report significance as: ***=99.9%, **= 99%, *= 95%. *Cases increment* is employed only in the linear regression in place of *new cases*, on the rightmost table. Positive coefficients represent higher mobility flows associated with higher covariates.

The second wave period model suggests consistent correlates with respect to the first wave model, namely labour structure, urbanization, municipality development, baseline period mobility network metrics, i.e., peripherality (*inbound path-length*), outbound trips per capita (*out-strenght*) and spatial autocorrelation. However, there are some differences between the two waves periods correlates: epidemiological variables, clustering and betweenness centrality are not statistically significant in the second wave, see the second column in Table 2.

Differences across waves

We aim to define the factors associated with the altered population response in the second wave with respect to the first wave, hence describing behavioral changes in response to repeated interventions. To approach this question, we employed a linear regression to explain the relative change of outgoing mobility observed during the second wave with respect to the first wave $\delta^2 M_i$ (see Methods). Here, we replaced the variable *new cases* with *cases increment*, *i.e.* to account for the relative change of cases incidence across waves.

The model achieves an adjusted $R^2 = 0.49$ and a statistically significant Kendall’s Tau coefficient of $\tau_k = 0.38$.

Our findings evidence that, with respect to the first wave, in the second wave period:

- higher mobility is observed in the municipalities with higher development index (*IDC*) and more active population employed in the tertiary sector;
- lower mobility is associated with higher urbanization indices, higher population, higher percentage of women, and higher age profiles.

Interestingly, we do not observe a significant role played by the increment of cases incidence.

Network resilience

The analysis carried on in the previous section shows a wide overlap of factors associated with mobility reductions and a significant role played by network metrics computed on the baseline mobility network. These quantities are static in time and refer to the configuration of the pre-interventions mobility network. Their significance thus suggests a remarkable resilience of the mobility network structure that we investigated by focusing on the change of mobility hotspots and origin-destination flows across the two waves periods.

Hotspots and traveling probabilities analyses

To compare the node features of the two networks, *i.e.* first and second wave mobility networks, we defined as hotspots the municipalities with the highest outbound mobility flows in each of the three periods using the Loubar method [47] (see Supplementary Section *Hotspots and traveling probabilities definition*). In each period, we defined three levels of hotspots ranked by their (decreasing) mobility outflows and subdivided the municipalities into three sets. For each level, we adopted the Jaccard similarity index J to compare the overlapping hotspots across the three periods. The results are summarized in Figure 2. The results evidence a large overlap at all three levels for all three periods. Interestingly, the hotspot configuration appears to be significantly stable between the first and the second wave, suggesting a significant correlation in the network structure.

To compare the link features of the two networks, we defined the probabilities of traveling from any municipality i to j as $p_{ij,P} = \frac{M_{ij,P}}{\sum_{k \neq i} M_{ik,P}}$, where $P \in \{b, f, s\}$, *i.e.* baseline, first or second wave period. Figure 3a,b shows that the highest probability routes, on the top right of the plots, are highly correlated across the three periods, and hence, the probability of traveling over the major routes out of municipalities in Chile is highly similar across periods. On the other hand, minor routes, laying on the bottom left corner of plots, are characterized by lower flows and show high differences across waves.

Spatial invasion modeling

As a proof of concept, we run an epidemic model to simulate the spatial invasion of an infectious disease arriving at Santiago’s airport on both the first and the second wave mobility networks. The model is a susceptible-infected (SI) model, where locations can only get infected once, and the probability of invasion depends on the mobility flows between areas (see Supplementary Section *Spatial invasion model*). We register the average arrival time of the disease at the municipality level obtained by running $n_s = 500$ simulations and show the comparison for the two waves mobility networks. In Fig. 3c,d, we show how structural similarities in the two epidemic waves mobility networks do not affect sensibly the outcomes of the predicted arrival times at municipalities. In Figure 3c, we observe a high correlation between arrival times of the first 14 days of simulations, which reflects the good correlation of the highest traveling probabilities p_{ij} in Figure 3a,b. On the other hand, the uncorrelated arrival times in the third week of simulations, in the top right corner of Figure 3c, reflect the higher degree of variability between minor

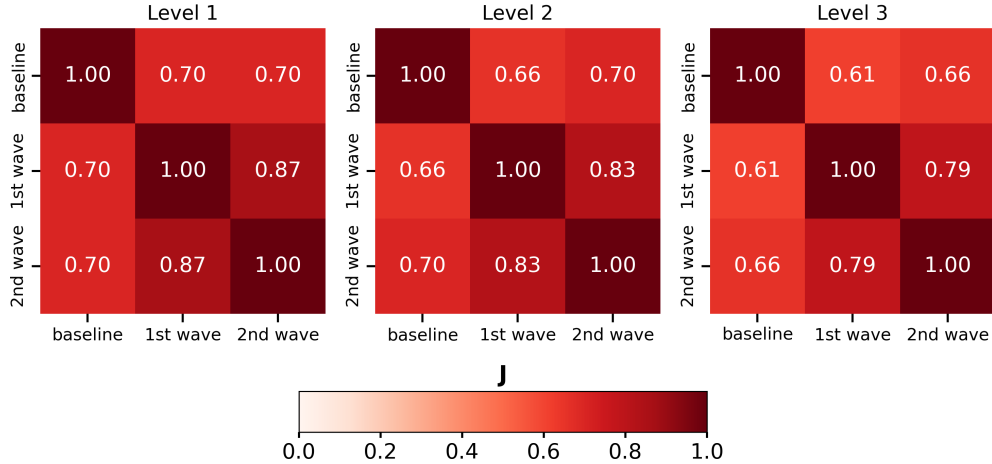


Figure 2: **Resilience of mobility hotspots across epidemic waves in Chile.** Heatmaps showing the Jaccard similarity J for three hotspot levels across the three periods, i.e., baseline, first, and second wave. Level increases from left to right, with Level 1 encoding *comunas* with the highest mobility flows.

routes in the first and second waves, i.e. the lowest traveling probabilities p_{ij} from any *comuna* i , shown in Figure 3a,b. This result highlights how the main routes of mobility between comunas were preserved well across the two waves, while the highest level of variability was registered in the secondary routes, representing a lower share of outbound travels from municipalities. As a sensitivity test, we performed the same simulation over a dynamic version of the mobility networks, in which the two waves networks account for the daily flows between municipalities (see Supplementary Section *Hotspots and traveling probabilities definition*). In Figure 3e,f, we show how results prove robust for temporal aggregation.

Validity of results in further countries

To check for the validity of our findings regarding the resilience of the mobility network across repeated interventions during the Covid-19 pandemic, we repeated the same methodology and analyses on the Spanish dataset and recovered consistent results for the Spanish case study in the three periods analogously defined (see Supplementary Section *Spanish network resilience*). In Supplementary Figure S1, we found a high overlap of mobility hotspots across the three periods, specifically with all Jaccard indexes above 60%, while in Supplementary Figure S2, we found a high correlation of traveling probabilities from Spanish municipalities, with Spearman correlations above $S_r = 0.89$ between first and second waves networks and $S_r = 0.92$ between second wave and baseline networks. Note that Spain counts with a higher number of municipalities with respect to Chile, 8132 vs 346 respectively, meaning that results are robust to different spatial configurations of the mobility network.

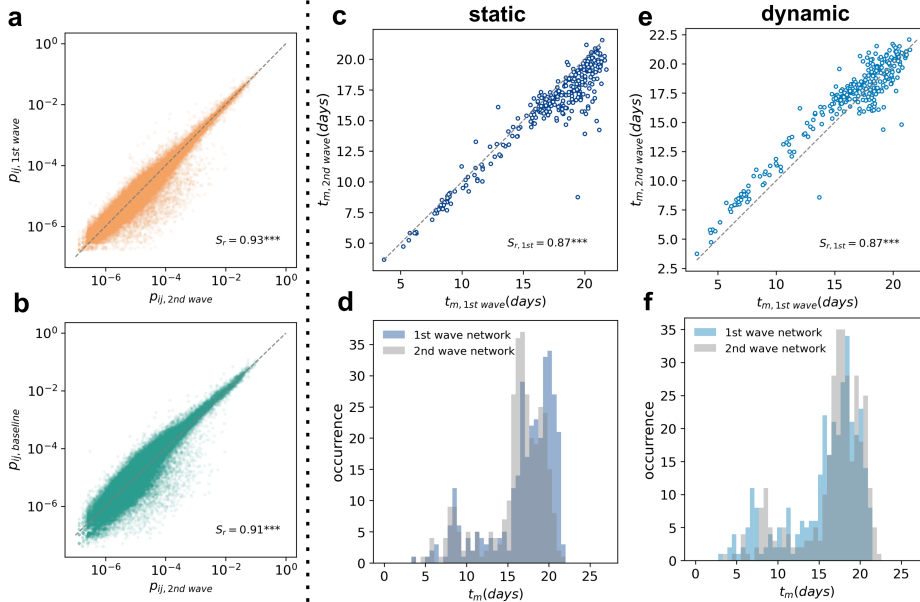


Figure 3: **Epidemic modeling on Chile’s two waves mobility networks.** (a) Traveling probabilities p_{ij} computed from the first wave network against those computed on the second wave network. (b) Traveling probabilities p_{ij} computed from the second wave network against those computed on the baseline network. The grey dashed line is the identity diagonal. The quantity S_r denotes the Spearman’s correlation coefficient computed on traveling probabilities. (c) Average arrival times t_m at municipalities resulted from the epidemic model run on the first and second wave static networks and (d) their distribution in time. (e) Average arrival times t_m at municipalities resulted from the epidemic model run on the first and second wave dynamic networks and (f) their distribution in time. The dashed grey line is the identity diagonal, and S_r is Spearman’s correlation coefficient computed between the two modeled average arrival times.

Discussion

We focused on the municipality-level mobility response to COVID-19 first and second-wave interventions in Chile, where we observed consistent factors associated with post-intervention mobility reduction across the two periods. These factors included network metrics encoding mobility patterns from the baseline pre-interventions period. This provides evidence that both mobility networks resulting from two separate interventions in two periods share similar structural aspects. We looked into the structural features of the two periods’ mobility networks and found that, despite changes in the behavioral response to interventions associated with specific demographic profiles, the two networks exhibited strong structural similarities. We characterized the similarity between the mobility networks of the first and second COVID-19 waves in Chile in terms of mobility hotspots overlap to account for node features and traveling probabilities correlations to account for the link features of the network. We expanded our analysis to the Spanish case study. By leveraging an open mobility dataset provided by the Spanish Ministry of Transportation [35, 36], we reproduced our analyses on the Spanish case study in the three periods analogously defined (baseline, first, and second wave). Our approach proved robust since we observed strong structural similarities between the mobility network of the second and first waves in Spain.

This resilience suggests that certain areas and routes are critical to explaining mobility despite varying restrictions and changes in public behavior. This has strong implications for epidemic modeling: since the major mobility routes are preserved across waves, they encode preferential pathways of spatial invasion, as proved by the essentially unchanged disease arrival times predicted by the model on the two periods networks. This finding adds to previous knowledge on the impact of mobility network heterogeneity on the predictability of disease spread at international level [48], in which major air travel routes determine a higher probability of spatial invasion. Observing a resilient mobility network at sub-national level, hence preserving major traveling probabilities across interventions, yields high predictability of spatial invasion patterns within the country beyond the initial epidemic phase. This observation can be exploited

to design *a priori* sentinel locations for epidemic surveillance of new strains, which represent the most at-risk of invasion locations in the country.

The spatial lag models reveal several key factors associated with mobility reduction during the first and second waves. Our analysis recovers some known relations already observed in the literature, such as the role of the labour structure [7], the urbanization level, active population, and local incidence [9].

Unlike previous studies, our modeling approach accounts for network metrics of municipality centrality in the baseline mobility network, which play a significant role in the population response to interventions in both waves. The positive correlation between mobility reductions and betweenness centrality suggests that the most central municipalities were also the most responsive to interventions. This is relevant because these municipalities are likely the most important in the long-range disease spread, hence playing as bottlenecks for invasion patterns. Lower mobility reductions are instead associated with higher clustering – hence pertaining to groups of densely connected interdependent municipalities –, higher inbound path length – hence peripheral *comunas* –, and with higher amount of trips per capita. This behavior can be attributed to peripheral locations with a higher economic dependency on neighboring municipalities in granting essential services to the population. During the second wave, besides the still determinant socio-economic variables, the only network significant correlates were the inbound path length and the per capita out-strength: peripheral municipalities with typically higher trips per capita had lower mobility reductions than others.

Our analyses further show the key differences in several variables when explaining the mobility variations between the first and second waves. Factors like age, gender, and population did not impact the post-intervention mobility change with respect to the baseline, but they were associated with a change in response in the second wave with respect to the first. Scarcely populated rural and peripheral areas, with a higher development index that are more populated by men of younger age exhibited higher mobility levels in the second wave with respect to the first wave. This indicates that dynamic population response to repeated interventions may be more strongly associated with certain demographic profiles rather than being common to the overall population.

Finally, the study finds significant spatial autocorrelation in mobility responses. This suggests that municipalities did not act or react independently to interventions but were influenced by neighboring areas. This observation underscores the importance of considering spatial dependencies in pandemic response strategies.

Our work shows that, despite population behavioral change to repeated interventions in areas with specific demographic profiles, centrality metrics, and clustering in the pre-intervention mobility network, urbanization, development, and labour structure, the overall mobility network exhibits relatively high resilience to shocks driven by NPIs. From a public health perspective, this resilience can be exploited to improve surveillance and inform interventions with historical mobility data, predicting areas at the highest invasion risk and allowing efficient allocation of resources to anticipate local outbreaks. These findings have strong implications for pandemic preparedness since, in this context, data readiness can be built without depending on real-time data streams.

Limitations

In this study, we did not consider local incidence stratified by demographic traits, which could have altered the population response of specific groups in the two waves.

While the mobility network we studied for the three periods, i.e. baseline, first, and second waves, is the result of an average over the first month post-interventions weekly flows, mobility is a dynamic process that can exhibit local, both spatially and temporally, fluctuations due to local holidays, seasonality, weather events, and regional climate. We chose to average weekly flows of four weeks post-interventions to minimize the effect of any of these factors on our analyses. In 3e,f, we prove how our results are robust to temporal aggregation of mobility flows, i.e., considering the original dynamic network of daily mobility flows.

This study did not consider variables related to Chilean climate regions. Further research is needed to account for climate impact on the resulting population response to NPIs.

Data availability statement

Data regarding socio-demographic variables at municipality level in Chile are publicly available [37]. Raw mobility data at municipality level from Chile are not publicly available due to privacy reasons, for more information see [49]. Analysis of the anonymised mobile phone data was performed on the mobile operator’s systems without transferring it outside. Only aggregated mobility patterns across municipalities were provided to researchers outside Chile, and only these have been used for the results presented here. Mobility data aggregated at municipality level from Spain are publicly available [36].

Acknowledgements

P.C.,K.K.,L.F.,L.D., N.G., M.M. acknowledge support from the Lagrange Project of the Institute for Scientific Interchange Foundation (ISI Foundation) funded by Fondazione Cassa di Risparmio di Torino (Fondazione CRT). This research was supported by FONDECYT Grant N°1221315 to Leo Ferres. L.D. further acknowledges support from Fondation Botnar (EPFL COVID-19 Real Time Epidemiology I-DAIR Pathfinder). M.M. acknowledges support from the Horizon Europe project VERDI (101045989) as well as from the EOSC project SIESTA (101131957).

Authors contributions

Research design: M.M., N.G., L.D.; Data collection: L.F., P.C.; Data analysis: P.C., M.M.; Research coordination: M.M.; First draft writing: P.C., M.M., N.G., K.K.; All authors reviewed and approved the manuscript.

Conflict of interest

The authors declare no conflict of interest.

References

- [1] Moritz UG Kraemer, Adam Sadilek, Qian Zhang, Nahema A Marchal, Gaurav Tuli, Emily L Cohn, Yulin Hswen, T Alex Perkins, David L Smith, Robert C Reiner Jr, et al. Mapping global variation in human mobility. *Nature Human Behaviour*, 4:800–810, 2020.
- [2] Lorenzo Lucchini, Simone Centellegher, Luca Pappalardo, Riccardo Gallotti, Filippo Privitera, Bruno Lepri, and Marco De Nadai. Living in a pandemic: changes in mobility routines, social activity and adherence to covid-19 protective measures. *Scientific reports*, 11:24452, 2021.
- [3] Corrine W Ruktanonchai, Shengjie Lai, Chigozie E Utazi, Alex D Cunningham, Patrycja Koper, Grant E Rogers, Nick W Ruktanonchai, Adam Sadilek, Dorothea Woods, Andrew J Tatem, et al. Practical geospatial and sociodemographic predictors of human mobility. *Scientific reports*, 11:15389, 2021.
- [4] David Holtz, Michael Zhao, Seth G Benzell, Cathy Y Cao, Mohammad Amin Rahimian, Jeremy Yang, Jennifer Allen, Avinash Collis, Alex Moehring, Tara Sowrirajan, et al. Interdependence and the cost of uncoordinated responses to covid-19. *Proceedings of the National Academy of Sciences*, 117:19837–19843, 2020.
- [5] Nicola Perra. Non-pharmaceutical interventions during the COVID-19 pandemic: A review. *Physics Reports*, 2021.
- [6] Benjamin M Althouse, Brendan Wallace, BKM Case, Samuel V Scarpino, Antoine Allard, Andrew M Berdahl, Easton R White, and Laurent Hébert-Dufresne. The unintended consequences of inconsistent closure policies and mobility restrictions during epidemics. *BMC Global and Public Health*, 1:28, 2023.
- [7] Nicolò Gozzi, Michele Tizzoni, Matteo Chinazzi, Leo Ferres, Alessandro Vespignani, and Nicola Perra. Estimating the effect of social inequalities on the mitigation of covid-19 across communities in santiago de chile. *Nature communications*, 12:2429, 2021.

- [8] Samuel Heroy, Isabella Loaiza, Alex Pentland, and Neave O’Clery. Covid-19 policy analysis: labour structure dictates lockdown mobility behaviour. Journal of the Royal Society Interface, 18:20201035, 2021.
- [9] Eugenio Valdano, Jonggul Lee, Shweta Bansal, Stefania Rubrichi, and Vittoria Colizza. Highlighting socio-economic constraints on mobility reductions during covid-19 restrictions in france can inform effective and equitable pandemic response. Journal of travel medicine, 28:taab045, 2021.
- [10] Duygu Balcan, Hao Hu, Bruno Goncalves, Paolo Bajardi, Chiara Poletto, Jose J Ramasco, Daniela Paolotti, Nicola Perra, Michele Tizzoni, Wouter Van den Broeck, et al. Seasonal transmission potential and activity peaks of the new influenza a (h1n1): a monte carlo likelihood analysis based on human mobility. BMC medicine, 7:1–12, 2009.
- [11] Paolo Bajardi, Chiara Poletto, Jose J Ramasco, Michele Tizzoni, Vittoria Colizza, and Alessandro Vespignani. Human mobility networks, travel restrictions, and the global spread of 2009 h1n1 pandemic. PloS one, 6:e16591, 2011.
- [12] Michele Tizzoni, Paolo Bajardi, Adeline Decuyper, Guillaume Kon Kam King, Christian M Schneider, Vincent Blondel, Zbigniew Smoreda, Marta C González, and Vittoria Colizza. On the use of human mobility proxies for modeling epidemics. PLoS computational biology, 10:e1003716, 2014.
- [13] Mattia Mazzoli, Emanuele Pepe, David Mateo, Ciro Cattuto, Laetitia Gauvin, Paolo Bajardi, Michele Tizzoni, Alberto Hernando, Sandro Meloni, and José J Ramasco. Interplay between mobility, multi-seeding and lockdowns shapes covid-19 local impact. PLoS computational biology, 17:e1009326, 2021.
- [14] Chiara E Sabbatini, Giulia Pullano, Laura Di Domenico, Stefania Rubrichi, Shweta Bansal, and Vittoria Colizza. The impact of spatial connectivity on npis effectiveness. BMC Infectious Diseases, 24:21, 2024.
- [15] Caroline O Buckee, Satchit Balsari, Jennifer Chan, Mercè Crosas, Francesca Dominici, Urs Gasser, Yonatan H Grad, Bryan Grenfell, M Elizabeth Halloran, Moritz UG Kraemer, et al. Aggregated mobility data could help fight covid-19. Science, 368:145–146, 2020.
- [16] Laura Di Domenico, Giulia Pullano, Chiara E Sabbatini, Pierre-Yves Boëlle, and Vittoria Colizza. Impact of lockdown on covid-19 epidemic in île-de-france and possible exit strategies. BMC medicine, 18:1–13, 2020.
- [17] Nuria Oliver, Bruno Lepri, Harald Sterly, Renaud Lambiotte, Sébastien Deletaille, Marco De Nadai, Emmanuel Letouzé, Albert Ali Salah, Richard Benjamins, Ciro Cattuto, et al. Mobile phone data for informing public health actions across the covid-19 pandemic life cycle. Science advances, 6:eabc0764, 2020.
- [18] Laura Alessandretti. What human mobility data tell us about COVID-19 spread. Nature Reviews Physics, 4(1):12–13, 2022.
- [19] Serina Chang, Emma Pierson, Pang Wei Koh, Jaline Gerardin, Beth Redbird, David Grusky, and Jure Leskovec. Mobility network models of COVID-19 explain inequities and inform reopening. Nature, 589(7840):82–87, 2021.
- [20] Mark Jit, Kylie Ainslie, Christian Althaus, Constantino Caetano, Vittoria Colizza, Daniela Paolotti, Philippe Beutels, Lander Willem, John Edmunds, Baltazar Nunes, et al. Reflections on epidemiological modeling to inform policy during the covid-19 pandemic in western europe, 2020–23: Commentary reflects on epidemiological modeling during the covid-19 pandemic in western europe, 2020–23. Health Affairs, 42:1630–1636, 2023.
- [21] Giulia Pullano, Lucila G Alvarez-Zuzek, Vittoria Colizza, and Shweta Bansal. Characterizing US spatial connectivity: implications for geographical disease dynamics and metapopulation modeling. medRxiv, pages 2023–11, 2023.
- [22] Ciro Cattuto Stefaan Verhulst, Daniela Paolotti and Alessandro Vespignani. Outpacing Pandemics: Solving the First and Last Mile Challenges of Data-Driven Policy Making. <https://medium.com/data-policy/outpacing-pandemics-solving-the-first-and-last-mile-challenges-of-data-driven-policy-making-c7f8ef6662a4>, 2024.

- [23] Akhil Anil Rajput and Ali Mostafavi. Latent sub-structural resilience mechanisms in temporal human mobility networks during urban flooding. *Scientific Reports*, 13:10953, 2023.
- [24] Zizhen Xu and Shauhrat S Chopra. Interconnectedness enhances network resilience of multimodal public transportation systems for safe-to-fail urban mobility. *Nature communications*, 14:4291, 2023.
- [25] Frank Schlosser, Benjamin F Maier, Olivia Jack, David Hinrichs, Adrian Zachariae, and Dirk Brockmann. Covid-19 lockdown induces disease-mitigating structural changes in mobility networks. *Proceedings of the National Academy of Sciences*, 117:32883–32890, 2020.
- [26] Weiyu Li, Qi Wang, Yuanyuan Liu, Mario L Small, and Jianxi Gao. A spatiotemporal decay model of human mobility when facing large-scale crises. *Proceedings of the National Academy of Sciences*, 119:e2203042119, 2022.
- [27] Clodomir Santana, Federico Botta, Hugo Barbosa, Filippo Privitera, Ronaldo Menezes, and Riccardo Di Clemente. Covid-19 is linked to changes in the time–space dimension of human mobility. *Nature Human Behaviour*, 7:1729–1739, 2023.
- [28] Haiyan Liu, Jianghao Wang, Jian Liu, Yong Ge, Xiaoli Wang, Chi Zhang, Eimear Cleary, Nick W Ruktanonchai, Corrine W Ruktanonchai, Yongcheng Yao, et al. Combined and delayed impacts of epidemics and extreme weather on urban mobility recovery. *Sustainable Cities and Society*, 99:104872, 2023.
- [29] Federico Delussu, Michele Tizzoni, and Laetitia Gauvin. Evidence of pandemic fatigue associated with stricter tiered covid-19 restrictions. *PLOS Digital Health*, 1:e0000035, 2022.
- [30] Kenichi Kurita, Yuya Katafuchi, and Shunsuke Managi. Covid-19, stigma, and habituation: evidence from mobility data. *BMC Public Health*, 23:98, 2023.
- [31] Zhanwei Du, Lin Wang, Songwei Shan, Dickson Lam, Tim K Tsang, Jingyi Xiao, Huizhi Gao, Bingyi Yang, Sheikh Taslim Ali, Sen Pei, et al. Pandemic fatigue impedes mitigation of covid-19 in hong kong. *Proceedings of the National Academy of Sciences*, 119:e2213313119, 2022.
- [32] Presidente declara Estado de Excepción Constitucional de Catástrofe en todo el territorio nacional - Gob.cl. <https://www.gob.cl/noticias/presidente-declara-estado-de-excepcion-constitucional-de-catastrofe-en-todo-el-territorio-nacional/>.
- [33] Gobierno anunció Plan “Paso a Paso Nos Cuidamos” para el desconfiamento gradual en todo el país - División de Organizaciones Sociales. <https://organizacionesociales.gob.cl/gobierno-anuncio-plan-paso-a-paso-nos-cuidamos-para-el-desconfiamento-gradual-en-todo-el-pais/>.
- [34] Desde este lunes comienzan a regir las nuevas medidas para bajar la movilidad de la población - Gob.cl. <https://www.gob.cl/noticias/gobierno-anuncia-nuevas-medidas-mas-restrictivas-para-bajar-movilidad-de-la-poblacion/>.
- [35] Miguel Ponce-de Leon, Javier Del Valle, José María Fernandez, Marc Bernardo, Davide Cirillo, Jon Sanchez-Valle, Matthew Smith, Salvador Capella-Gutierrez, Tania Gullón, and Alfonso Valencia. COVID-19 Flow-Maps an open geographic information system on COVID-19 and human mobility for Spain. *Scientific Data*, 8:310, 2021.
- [36] Ministry of Transport, Mobility and Urban Agenda of Spain, MITMA. Open Data Movilidad 2020-2021. <https://www.transportes.gob.es/ministerio/covid-19/evolucion-movilidad-big-data/pendata-movilidad>.
- [37] Instituto Nacional de Estadística de Chile. Censo de poblacion y vivienda. <https://www.ine.gob.cl/estadisticas/sociales/censos-de-poblacion-y-vivienda/censo-de-poblacion-y-vivienda>.
- [38] Universidad Autónoma de Chile. Índice de desarrollo comunal. <https://www.uaautonoma.cl/noticias/indice-de-desarrollo-comunal-2020-refleja-altos-indices-de-desigualdad-en-el-desarrollo-comunal-de-chile/>.

- [39] Ministerio de Ciencia, Tecnología, Conocimiento e Innovación de Chile. Data repository of the Chilean Ministry of Science. <https://github.com/MinCiencia/>.
- [40] Departamento de Estadísticas e Información de Salud. Datos abiertos. <https://deis.minsal.cl/#datosabiertos>.
- [41] A.D. Cliff and J.K. Ord. Spatial Processes: Models and Applications. Pion, London, 1981.
- [42] Fuzzy contiguity matrix. https://pysal.org/libpysal/generated/libpysal.weights.fuzzy_contiguity.html.
- [43] Sergio J Rey and Luc Anselin. Pysal: A python library of spatial analytical methods. In Handbook of applied spatial analysis: Software tools, methods and applications, pages 175–193. Springer, 2009.
- [44] Luc Anselin. Spatial Econometrics: Methods and models. Kluwer, Dordrecht, 1988.
- [45] Spatial lag model. https://pysal.org/spreg/generated/spreg.ML_Lag.html#spreg.ML_Lag.
- [46] R. Anderson J. Hair and B. Babin. Multivariate Data Analysis. Prentice Hall, 7 edition, 2009.
- [47] Louail T. et al. From mobile phone data to the spatial structure of cities. Sci. Rep. 4, 5276, (2014).
- [48] Vittoria Colizza, Alain Barrat, Marc Barthélemy, and Alessandro Vespignani. The role of the airline transportation network in the prediction and predictability of global epidemics. Proceedings of the National Academy of Sciences, 103:2015–2020, 2006.
- [49] Luca Pappalardo, Giuliano Cornacchia, Victor Navarro, Loreto Bravo, and Leo Ferres. A dataset to assess mobility changes in chile following local quarantines. Scientific Data, 10(1), January 2023.

Supplementary Information
*Resilience of mobility network to dynamic population
response across COVID-19 interventions: evidences
from Chile*

Pasquale Casaburi^{1,2}, Lorenzo Dall’Amico¹, Nicolò Gozzi¹, Kyriaki Kalimeri¹, Anna Sapienza^{3,1},
Rossano Schifanella^{1,4}, T. Di Matteo^{2,5,6}, Leo Ferres^{7,1}, Mattia Mazzoli¹

¹ ISI Foundation, via Chisola 5, 10126 Turin, Italy

² Department of Mathematics, King’s College London, The Strand, London WC2R 2LS, UK

³ Università del Piemonte Orientale, Alessandria, Italy

⁴ Università degli Studi di Torino, Turin, Italy

⁵ Complexity Science Hub Vienna, Josefstädter Straße 39, 1080 Vienna, Austria

⁶ Centro Ricerche Enrico Fermi, Via Panisperna 89 A, 00184 Rome, Italy

⁷ Universidad del Desarrollo, Santiago de Chile, Chile

Contents

1	Network metrics	2
2	Hotspots and traveling probabilities definition	3
3	Municipality sample	4
3.1	Chilean municipalities	4
3.2	Spanish municipalities	4
4	Spanish mobility network resilience	5

1 Network metrics

To study the effect of the business-as-usual mobility network structure on the response of the Chilean municipalities to the pandemic, by using the weekly OD matrices for the two weeks in the baseline period $M_{ij,w}$, we built a weighted and directed network whose nodes are municipalities and whose edge weights $M_{ij,w}$ are the weekly flows from node i to node j in week w . From these networks, we extract six metrics: the per capita out(in)-strength, the average out(in)-bound path length, the clustering coefficient, and the betweenness centrality. First, for each node i we define the per capita out-strength and in-strength as:

$$S_{out,i,w} = \sum_j \frac{M_{ij,w}}{pop_i}, \quad (1)$$

$$S_{in,i,w} = \sum_j \frac{M_{ji,w}}{pop_i}. \quad (2)$$

To compute these quantities we divided by the municipality population pop_i to account for the heterogeneous population sizes, hence representing the weekly number of out-bound and in-bound trips per capita. We defined the weighted shortest path length connecting i to any other node j in the network:

$$L_{ij,w} = \sum_{k \in s.p.(i,j)} \frac{1}{M_{ik,w}}, \quad (3)$$

where the sum is carried out over all nodes k belonging to the shortest path connecting i and j and distance is measured as the inverse of the trips between them. This quantity is then averaged over all routes in which node i is the origin (destination) to obtain the variable $\langle l_{out,i,w} \rangle$ ($\langle l_{in,i,w} \rangle$):

$$\langle l_{out,i,w} \rangle = \frac{1}{(N-1)} \sum_{j \neq i} L_{ij,w}, \quad (4)$$

$$\langle l_{in,i,w} \rangle = \frac{1}{(N-1)} \sum_{j \neq i} L_{ji,w}, \quad (5)$$

where N is the total number of nodes in the network. Lastly, we considered the betweenness

centrality of each node and its clustering coefficient as commonly defined for weighted directed networks [1]:

$$c_{i,w} = \frac{[M_w^{1/3}] + (M_w^T)^{1/3}]_{ii}^3}{2[d_{i,w}^{tot}(d_{i,w}^{tot} - 1) - 2d_{i,w}^{\leftrightarrow}]}, \quad (6)$$

where $M_w^{1/3} = \{M_{ij,w}^{1/3}\}$ is the matrix of all edge weights raised to the power 1/3, $d_{i,w}^{tot}$ is the sum of in-degree and out-degree of node i and $d_{i,w}^{\leftrightarrow}$ is the number of bilateral edges between i and its neighbors. Since the baseline covers two weeks, we computed them in both weeks independently, and then we averaged over the two values.

2 Hotspots and traveling probabilities definition

We define out-bound mobility hotspots among the municipalities following the methodology outlined in [2]. We use the weekly average mobility network $\bar{M}_{ij,P}$, with $P = b, f, s$, previously defined in the baseline, first, and second wave respectively, and we compute for every municipality i the total number of outbound mobility $\bar{M}_{i,P}$ occurring in the period P as:

$$\bar{M}_{i,P} = \sum_{j \neq i} \bar{M}_{ij,P}, \quad (7)$$

we rank them in ascending order $\bar{M}_{1,P} < \bar{M}_{2,P} < \dots < \bar{M}_{N,P}$ and assign them a fractional rank $F_{i,P} = i/N$. For each period p we build the Lorenz curve by placing on the x-axis the fractional rank $F_{i,P}$ and on the y-axis the cumulative number of municipalities outbound trips $L_{i,P}$ with:

$$L(i, P) = \frac{\sum_{j=1}^i \bar{M}_{j,P}}{\sum_{j=1}^N \bar{M}_{j,P}} \quad (8)$$

We consider as hotspots only those municipalities with a fractional rank greater than a certain threshold F^* as the intersection point between the tangent of the Lorenz curve at $F = 1$ and the x-axis [2]. We can further define hotspots of lower levels by eliminating the previously designed ones and repeating this process in the remaining municipalities. The higher the hotspots ranking the lower the mobility considered, hence we only consider 3 levels.

To account for the mixing of i and j comunas, we define the weekly average traveling probabilities

to travel from any municipality i to j in any of the three periods P as:

$$p_{ij,P} = \frac{\bar{M}_{ij,P}}{\sum_{k \neq i} \bar{M}_{ik,P}} \quad (9)$$

where the sum on k runs on all destinations in order to have $\sum_j p_{ij} = 1$ and $P \in \{b, f, s\}$ defines the first or second wave period. These are shown in Fig.3a-d in the main text. In order to perform a sensitivity test, we also realize a dynamic version of the traveling probabilities, which now encode daily traveling probabilities obtained from the original dataset without weekly aggregation nor averaging, hence yielding:

$$p_{ij,d,P} = \frac{M_{ij,d,P}}{\sum_{k \neq i} M_{ik,d,P}} \quad (10)$$

where d encodes the day of the period P . These are employed in the sensitivity analysis of the spatial invasion model, whose results are shown in Fig.3e,f of the main text.

3 Municipality sample

3.1 Chilean municipalities

In Chile, there are 346 municipalities, of which 11 contain few cell towers (i.e., < 10) in them, and others are scarcely populated, e.g., islands. Moreover, in our work, we consider spatial auto-correlation, and we strictly use geographical adjacency to inform the weighted matrix of municipalities' proximity. For the sake of representativeness and consistency, the above municipalities were excluded from our analysis. Finally, for the statistical analysis carried out in the Results section we considered 319 municipalities, or *comunas*, in mainland Chile.

3.2 Spanish municipalities

In Spain there are overall 8132 municipalities, many of these are rural areas with low population density and are not covered by mobile phone antennas. This dataset represents mobility between 2205 municipalities, in which small and rural municipalities that are not covered by mobile network antennas were aggregated together [3].

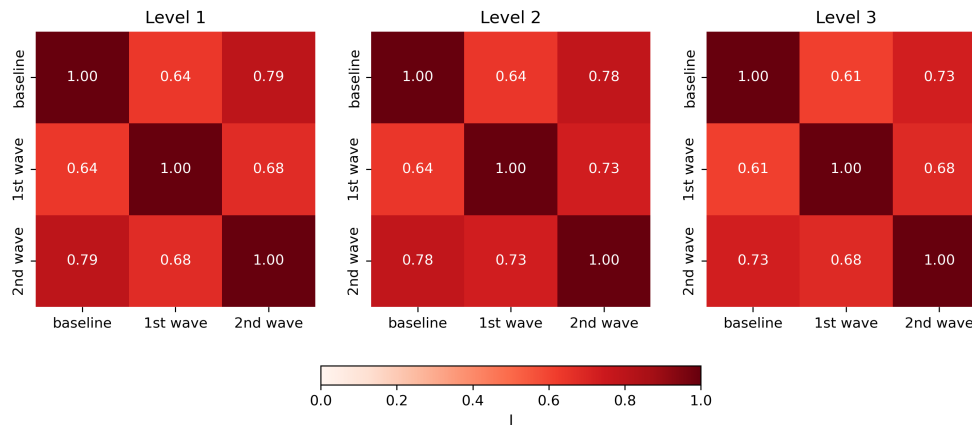
4 Spanish mobility network resilience

On March 14, 2020, the Spanish Government declared the first State of Alarm[4], which had critical repercussions on national mobility, such as the limitations of individual mobility that did not regard essential activities. On April 28, 2020, the Spanish Ministry of Health released regional measures of interventions towards the gradual reopening and recovery of all activities and mobility. These measures encoded a tiered system constituted of four phases, allowing for recovery of mobility at provincial and regional levels depending on specific epidemiological parameters. The summer period of 2020 exhibited low transmission in the country, however cases incidence resurgences were detected during the month of September, and cases kept increasing during the fall, culminating on October 25, 2020, on the Governmental declaration of the second State of Alarm [4]. Following this succession of events and analogously to the Chilean case study, we defined the baseline period as the week starting on February 21, 2020, the first wave as the four weeks following March 14, 2020, and the second wave as the four weeks following October 25, 2020.

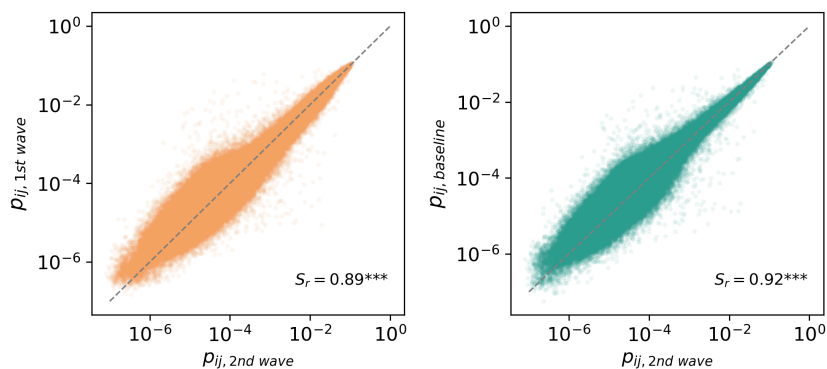
Finally, we reproduced the same analyses performed in the main text by analyzing the mobility network across the three time periods, this time over the Spanish mobility network.

In Supplementary Figure 2 we show the overlap of hotspots of the same level across the three periods. We measured the overlap among hotspots of the same level using the Jaccard index.

In Supplementary Figure 1 we show the correlation plot for the weekly average traveling probabilities measured in the three periods, on the left the comparison between the first and second wave periods, on the right the comparison of the baseline period traveling probabilities with those measured in the second wave.



Supplementary Figure 1: **Resilience of mobility hotspots across epidemic waves in Spain.** Heatmaps showing the Jaccard similarity J for three hotspot levels across the three periods, i.e., baseline, first, and second wave in Spain. Level increases from left to right, with Level 1 encoding the highest mobility flows.



Supplementary Figure 2: **Transition probabilities across waves in Spain.** (a) Transition probabilities p_{ij} computed from the first wave network against those computed on the second wave network. (b) Transition probabilities p_{ij} computed from the second wave network against those computed on the baseline network. The grey dashed line is the identity diagonal. The quantity S_r denotes Spearman's correlation coefficient computed between the two modeled average arrival times.

References

- [1] G Fagiolo. Clustering in complex directed networks. *Phys. Rev. E* 76, (2007).
- [2] Louail T. et al. From mobile phone data to the spatial structure of cities. *Sci. Rep.* 4, 5276, (2014).

- [3] Miguel Ponce-de Leon, Javier Del Valle, José María Fernández, Marc Bernardo, Davide Cirillo, Jon Sanchez-Valle, Matthew Smith, Salvador Capella-Gutierrez, Tania Gullón, and Alfonso Valencia. COVID-19 Flow-Maps an open geographic information system on COVID-19 and human mobility for Spain. *Scientific Data*, 8:310, 2021.
- [4] Observatorio del transporte y la logística en España. Medidas de restricción de la movilidad aplicadas en España. https://otle.transportes.gob.es/inform_covid/es/2020/21a-limitacion-de-la-movilidad-como-medio-para-controlar-la-propagacionde-la-pandemia/22-medidas-de-restriccionde-la-movilidad-aplicadas-en-espana.